

# Performance Analysis of Fractional Wireless Power Transfer Systems via Scattering Parameters

Arshaque Ali 

*School of Information Technology,  
Engineering, Mathematics and Physics  
The University of the South Pacific  
Suva, Fiji Islands.  
arshaqueabraali@outlook.com*

Utkal Mehta 

*School of Information Technology,  
Engineering, Mathematics and Physics  
The University of the South Pacific  
Suva, Fiji Islands.  
utkal.mehta@usp.ac.fj*

**Abstract**—Analyzing fractional-order wireless power transfer (WPT) systems through scattering parameters reveals several advantages over their classical counterparts. Compared to the fixed value in classical systems, the most notable improvement is the variable nature of the critical coupling coefficient in fractional systems. This contrasts with the classical system, which shows optimal performance only under near-perfect coupling conditions and within a narrow frequency band around the resonant frequency. The efficiency analysis reveals that the fractional system maintains a higher transfer efficiency at lower coupling coefficients by leveraging higher frequency operations, a capability not present in classical WPT systems. The ability to optimise performance through frequency adjustment rather than physical coupling modifications represents a significant advancement in wireless power transfer technology.

**Index Terms**—Fractional order elements; Wireless power transfer; Fractional modeling; Coupling coefficient; Resonant frequency.

## I. INTRODUCTION

As WPT systems evolve in complexity, the need for accurate modeling and analysis techniques to optimise performance and efficiency becomes increasingly important. Modeling WPT systems enables engineers to predict and improve efficiency, robustness, and adaptability, especially for emerging applications such as electric vehicle charging [1], biomedical implants [2], and consumer electronics. An important step in accurately understanding the behaviour of electrical systems is the development of a mathematical model that allows evaluation based on specified system parameters. Although there exist mathematical models for fractional WPT systems (fWPT) [3]–[5] that provide for a more accurate analysis compared to classical models, studies that involve them have not fully captured and explored the dynamics of the system. The phenomena involving frequency bifurcation (aka frequency splitting) and the concept of the critical coupling coefficient has been explored in great detail in a study by Shu et al. [6]. The critical coupling coefficient,  $k_{critical}$  marks the transition between the undercoupled and overcoupled regimes. It represents the coupling strength at which the maximum power transfer efficiency is achieved. This phenomenon is crucial for system optimisation, as an operating frequency near  $k_{critical}$  often yields the best performance. The analysis [6]

shows that the series-series fractional system can achieve a regulated frequency bifurcation behaviour, increased working range, and enhanced power output by simply adjusting the fractional orders.

On the other hand, our study presents formulated equations that incorporate these dynamics into fractional modeling equations of a series-parallel WPT system by taking advantage of the scattering ( $S$ ) parameters of the two-port coil antenna system. The use of  $S$  parameters, more specifically the  $S_{21}$  parameter, serves as an important parameter for analysing the behaviour of WPT systems, offering insight into power transfer efficiency, impedance matching, and system stability [7]. Examination of these parameter variations with changes in coupling strength and operating frequency enables a deeper understanding of the dynamics of the fWPT system and facilitates the identification of optimal operating conditions of any given fractional or classical WPT system.

### A. Brief Description of Elements with Fractional Impedances

Elements with Fractional Impedances (EFIs) represent an innovative class of electrical components that extend the traditional concept of circuit elements beyond the integer-order domain. These elements, characterised by non-integer order behaviour, have gained significant attention in recent years due to the ability to accurately model certain physical phenomena and systems [8]–[10]. EFIs are mathematically described by fractional-order differential equations, where the order of differentiation or integration is not restricted to integer values. EFIs can be further classified into two distinct categories: Fractional-order capacitors (FOCs) and fractional-order inductors (FOIs) [11]. Within these distinct categories, their realisation can be achieved by selecting the fractional order, denoted by  $\alpha$  for FOCs and  $\beta$  for FOIs. For orders between 0 and 1, the EFI exhibits a positive resistance and consumes power, similar to classical, integer-order components. However, if the order is greater than 1, the EFIs inherit a negative resistance property and start to supply power. The impedance of EFIs is typically expressed as

$$Z(s) = K s^\alpha \quad (1)$$

where  $s$  is the complex frequency variable,  $K$  is a constant, and  $\alpha$  is a non-integer value, usually between 0 and 1. The unique properties of EFIs, such as a constant phase angle over a wide frequency range, make them particularly useful in modeling systems with memory effects, distributed parameters, or complex diffusion processes [12]. The applications of EFIs span various fields, including viscoelastic material characterisation, electrochemical system analysis, biological tissue modeling, and wireless power transfer systems [13]. In the context of wireless power transfer, EFIs have shown promise in improving the accuracy of coupling models and enhancing the efficiency of power transmission across varying distances and orientations [14]. Although ideal fractional-order elements do not exist as discrete components, an approximation can be performed using networks of conventional resistors and capacitors or realised through specialised materials and structures [15]. Recent advances in nanotechnology and material science have opened new avenues for the physical implementation of EFIs, another step closer to practical circuit applications [16]–[20].

### B. Mathematical Model of CEFI-based fWPT System

The fWPT Series-Parallel (S-P) topology forms three loops, as shown in Figure 1. The circuit can comprise a pair of fractional-order capacitors, one on each side of the system on the transmission and receiving sides of the system. For a system that has both fractional-order capacitors and fractional-order inductors, refer to [5] and [4] for the mathematical models of the Series-Series (S-S) and S-P fWPT topologies, respectively.

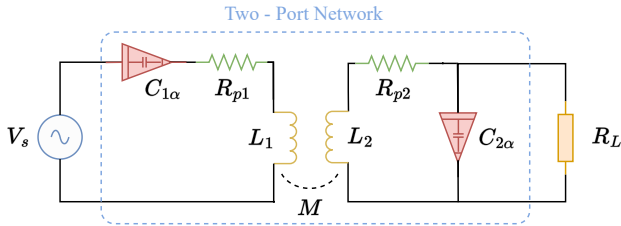


Fig. 1. S-P fWPT topology.

The application of Kirchhoff's voltage law (KVL) to the three loops yields 2 through 4. It should be noted that loops 1 and 2 exhibit mutual coupling, which is reflected in these equations.

$$V_s = I_1 (R_{p1} + Z_{C1} + Z_{L1}) + I_2 Z_M \quad (2)$$

$$0 = I_2 (R_{p2} + Z_{L2}) + Z_{C2} (I_2 - I_3) + I_1 Z_M \quad (3)$$

$$0 = Z_{C2} (I_3 - I_2) + I_3 R_L \quad (4)$$

where

- $V_s$  is an AC voltage source operating at the resonance frequency.

- $R_{p1}$  is the parasitic resistance component of the transmission coil.
- $R_{p2}$  is the parasitic resistance component of the receiving coil.
- $Z_{C1}$  is the equivalent impedance of the transmission side compensation capacitor.
- $Z_{C2}$  is the equivalent impedance of the reception side compensation capacitor.
- $Z_{L1}$  is the equivalent impedance of the transmission coil.
- $Z_M$  is the equivalent mutual impedance.
- $Z_{L2}$  is the equivalent impedance of the receiving coil.
- $R_L$  is the load resistance.
- $I_1$  is the current flowing in the transmission loop.
- $I_2$  is the current flowing in the first loop of the secondary side.
- $I_3$  is the current flowing in the second loop of the secondary side.

The impedances  $Z_{C1}$ ,  $Z_{C2}$ ,  $Z_{L1}$ ,  $Z_{L2}$ , and  $Z_M$  are defined by equations 5, where the subscript  $k \in 1, 2$  denotes the transmission side (1) and the reception side (2), respectively.

$$\begin{aligned} Z_{Ck} &= R_{Ck} - jX_{Ck} \\ Z_{Lk} &= R_{Lk} + jX_{Lk} \\ Z_M &= R_M + jX_M \end{aligned} \quad (5)$$

where

- $R_{Ck}$  and  $R_{Lk}$  are equivalent resistances of the fractional-order capacitor and inductor, respectively.
- $X_{Ck}$  and  $X_{Lk}$  are equivalent reactances of the fractional-order capacitor and inductor, respectively.
- $R_M$  and  $X_M$  are equivalent resistances and equivalent reactances of the mutual inductance, respectively.

These impedance components are defined by the relationships given in (6), while the equivalent impedance of the transmitter and receiver units is given by (7).

$$\begin{aligned} R_{Ck} &= \frac{1}{\omega^{\alpha_k} C_{k\alpha}} \cos \frac{\alpha_k \pi}{2}, \\ X_{Ck} &= \frac{1}{\omega^{\alpha_k} C_{k\alpha}} \sin \frac{\alpha_k \pi}{2}, \\ X_{Lk} &= \omega L_k, \\ R_M &= 0, \\ X_M &= \omega M. \end{aligned} \quad (6)$$

$$\begin{aligned} Z_1 &= R_{p1} + Z_{C1} + Z_{L1} \\ Z_2 &= R_{p2} + Z_{C2} - \frac{Z_{C2}^2}{Z_{C2} + R_L} \end{aligned} \quad (7)$$

Using equations (2) through (7), the currents flowing through fractional-order capacitors and classical inductors in both the transmitter and receiver circuits can be derived as per 8 - 11.

$$I_1 = \frac{Z_2 V_s}{\chi} \quad (8)$$

$$I_2 = -\frac{Z_M V_s}{\chi} \quad (9)$$

$$I_3 = \frac{Z_{C2}I_2}{Z_{C2} + R_L} \quad (10)$$

where,

$$\chi = Z_1Z_2 - (Z_M)^2 \quad (11)$$

The supply angular frequency, denoted by  $\omega_s$ , must be set to the resonance angular frequency ( $\omega_o$ ) for MRC and is determined by (12). The compensation capacitances required to achieve resonance at a desired frequency are also obtained from the same equation.

$$\omega_o = \alpha_k^{k+1} \sqrt{\frac{\sin \frac{\alpha_k \pi}{2}}{L_k C_k \sin \frac{\pi}{2}}} \quad (12)$$

For a system that uses a fractional order in the range of 0 to 1, the input power  $P_{in}$ , the output power  $P_{out}$  and the efficiency  $\eta$  can be calculated using (13)

$$\begin{aligned} P_{in} &= V_s |I_1| \\ P_{out} &= |I_3|^2 R_L \\ \eta &= \frac{P_{out}}{P_{in}} \times 100 \end{aligned} \quad (13)$$

While informative, the relationships in (13) are not optimal for quickly analysing the phenomena of  $k_{critical}$  and frequency bifurcation in fWPT systems. To better visualise and comprehend these effects, the scattering parameters must be incorporated into the analysis, allowing a more efficient and detailed system examination.

### C. Scattering Parameters

Scattering parameters, often denoted as *S-parameters*, are widely used in the analysis of two-port networks. A two-port network consists of a transmitting port and a receiving port. The S-parameters describe how signals are scattered or transmitted between these ports. For a generic two-port network, such as the one shown in Figure 2, the *S* parameter matrix is defined by (14).

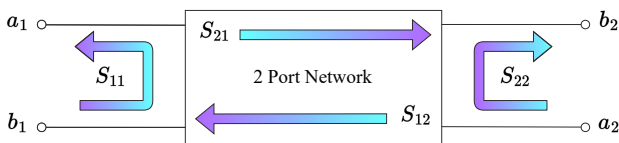


Fig. 2. S parameters of a two-port network

$$\begin{bmatrix} b_1 \\ b_2 \end{bmatrix} = \begin{bmatrix} S_{11} & S_{12} \\ S_{21} & S_{22} \end{bmatrix} \begin{bmatrix} a_1 \\ a_2 \end{bmatrix} \quad (14)$$

In this matrix,  $S_{11}$  represents the reflection coefficient for Port 1,  $S_{22}$  represents the reflection coefficient for Port 2,  $S_{21}$  represents the transmission coefficient from Port 1 to Port 2, and  $S_{12}$  represents the transmission coefficient from Port 2 to Port 1. The *S*-matrix for a two-port network is derived according to (18), using (15) and (17).

$$Z = \begin{bmatrix} Z_{11} & Z_{12} \\ Z_{21} & Z_{22} \end{bmatrix} \quad (15)$$

$$Z_0 = \begin{bmatrix} Z_{P1} & 0 \\ 0 & Z_{P2} \end{bmatrix} \quad (16)$$

$$F = \begin{bmatrix} \frac{1}{2\sqrt{\text{Re}\{Z_{P1}\}}} & 0 \\ 0 & \frac{1}{2\sqrt{\text{Re}\{Z_{P2}\}}} \end{bmatrix} \quad (17)$$

$$S = F(Z - Z_0^*)(Z + Z_0)^{-1}F^{-1} \quad (18)$$

where,

- $Z$  is the impedance matrix, formed from the impedances of the WPT system.
- $Z_{P1}$  and  $Z_{P2}$  are the reference impedances for Port 1 and Port 2 respectively.
- $Z_0$  is the reference impedance matrix.
- $F$  is the normalisation matrix formed from the reference impedance values.

For a two-port network with impedances as shown in (15), each S parameter is calculated using (19) - (22).

$$S_{11} = \frac{(Z_{11} - Z_0)(Z_{22} + Z_0) - Z_{12}Z_{21}}{(Z_{11} + Z_0)(Z_{22} + Z_0) - Z_{12}Z_{21}} \quad (19)$$

$$S_{12} = \frac{2Z_0Z_{12}}{(Z_{11} + Z_0)(Z_{22} + Z_0) - Z_{12}Z_{21}} \quad (20)$$

$$S_{21} = \frac{2Z_0Z_{21}}{(Z_{11} + Z_0)(Z_{22} + Z_0) - Z_{12}Z_{21}} \quad (21)$$

$$S_{22} = \frac{(Z_{11} + Z_0)(Z_{22} - Z_0) - Z_{12}Z_{21}}{(Z_{11} + Z_0)(Z_{22} + Z_0) - Z_{12}Z_{21}} \quad (22)$$

For WPT, the parameter  $S_{21}$ , represented as 21, is of great interest, as it quantifies the power transfer from the transmitting to the receiving coil and is directly related to the coupling. A higher  $S_{21}$  indicates stronger coupling and higher efficiency. Plotting the  $S_{21}$  parameter against  $k$  and  $f$  would reveal how  $k_{critical}$  varies with frequency, providing valuable information on the system's behaviour.

## II. NUMERICAL SIMULATION RESULTS

A numerical simulation of the CEFI-based fWPT system, depicted in Figure 1, was performed using MATLAB. The simulation used the system parameters specified in Table I, which were derived from empirical measurements obtained from the experimental setup. This approach ensures consistency and comparability between the simulated model and the physical system under investigation.

Before delving into the fractional WPT system analysis, it is necessary to set a benchmark of WPT system behaviour and observations using the classical WPT system.

TABLE I  
SIMULATION CIRCUIT PARAMETERS

Parameter	Value
$f_o$	130 kHz
$R_{p1}$	$0.1346\Omega$
$R_{p2}$	$0.1231\Omega$
$L_1$	$10.760\ \mu H$
$L_2$	$0.616\ \mu H$
$R_L$	$30\ \Omega$
$R_s$	$2.5\ \Omega$

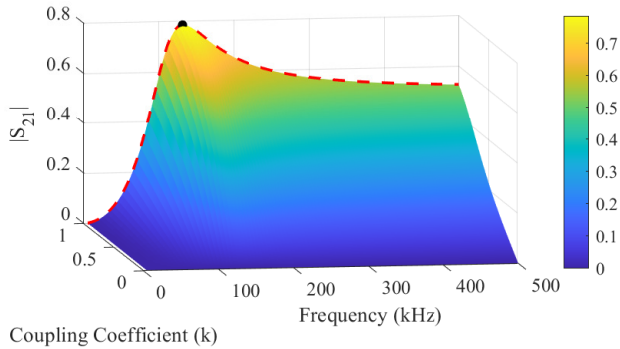


Fig. 3. Dependence of  $|S_{21}|$  on frequency and coupling coefficient.

1) *Classical WPT System*: Plotting  $|S_{21}|$  against  $k$  and  $f$  results in the surface plot shown in Figure 3.

$|S_{21}|$  exhibits strong frequency dependence, particularly at higher coupling coefficients. The maximum transmission occurs at the lower end of the chosen frequency bandwidth and high  $k$  values, with  $|S_{21}|$  reaching approximately 0.8. As frequency increases,  $|S_{21}|$  generally decreases, although a notable local maximum is observed around 80-160 kHz for highly coupled cases. This suggests a resonance effect in this frequency range. The red dashed line shows that the  $|S_{21}|$  value is affected by the frequency at  $k_{critical}$ . In this case,  $k_{critical}$  is clearly outlined as 1, which is the ideal coupled scenario. The black dot in the surface plot marks the point with the highest value of  $|S_{21}|$ , 0.787 with  $k = 1$  and  $f = 131.31\text{kHz}$ . This reveals that the design resonance frequency choice of 130kHz exhibits a higher  $|S_{21}|$  as desired, aligning with the system's optimal performance. At lower coupling coefficients ( $k < 0.2$ ),  $|S_{21}|$  remains relatively low in all frequencies, indicating weak transmission. The observed behaviour implies that optimal system performance may be achieved by carefully tuning both operating frequency and coupling strength. The plot of transfer efficiency against coupling coefficient and frequency, as shown in Figure 4 also resembles the same nature, with efficiency peaking around the point where the  $|S_{21}|$  parameter peaked. The efficiency variation is depicted using a colour gradient that transitions from dark blue for 0% to dark red for 100%.

The efficiency reaches its maximum of 90.61% at 121.21 kHz with  $k = 1$  as indicated by the black dot. As the coupling coefficient decreases, simulating an increase in the

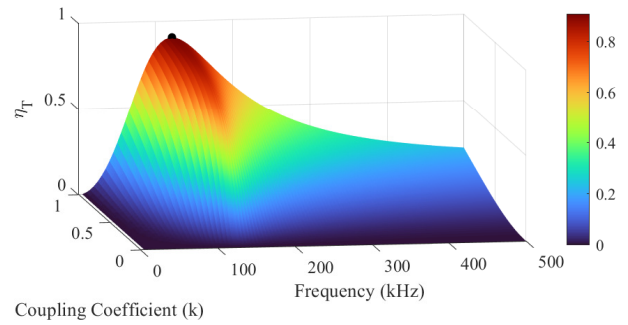


Fig. 4. Dependence of  $\eta_T$  on frequency and coupling coefficient.

transfer distance, the peak efficiency shifts toward 131.31 kHz. This shift aligns with the behaviour observed in the analysis of the  $S_{21}$  parameters. The frequency shift phenomenon is attributed to the system's transition from an overcoupled state to optimal coupling. In the overcoupled regime (high  $k$  values), the mutual inductance significantly impacts the impedance of the transmission and reception circuits, causing the efficiency peak to occur at a lower frequency. As  $k$  decreases, the system approaches critical coupling, and the maximum efficiency resonant frequency converges to the designed frequency of 131.31 kHz, depicted by the cyan dashed line in Figure 5.

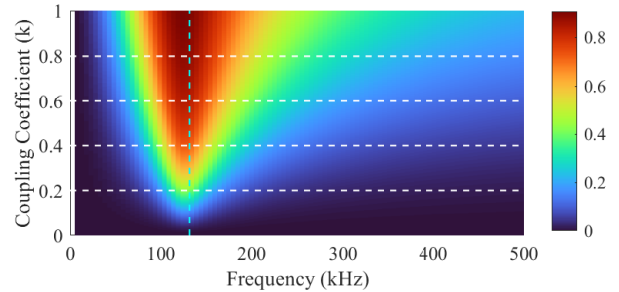


Fig. 5. X-Y view of Figure 4 nt.

The surface plot reveals a sharp efficiency peak at high coupling coefficients, indicating a narrow bandwidth for optimal operation. As  $k$  decreases, the efficiency not only reduces, but also exhibits a wider frequency response, suggesting a trade-off between the maximum achievable efficiency and the operating frequency range. It underscores the importance of adaptive frequency tuning to maintain high efficiency across different coupling scenarios.

2) *FOC-based Fractional WPT System*: Configuration 2 of the FOC fractional WPT system produces the surface plot shown in Figure 6.

In contrast to Figure 3, the introduction of an FOC of order 0.95 on the reception side positively alters the behaviour of  $|S_{21}|$  with respect to frequency. This new configuration reveals that  $k_{critical}$  now varies with frequency, rather than remaining constant. Notably, this shift allows for a more flexible system, where optimal coupling can be achieved at greater transfer distances simply by adjusting the operating frequency. This

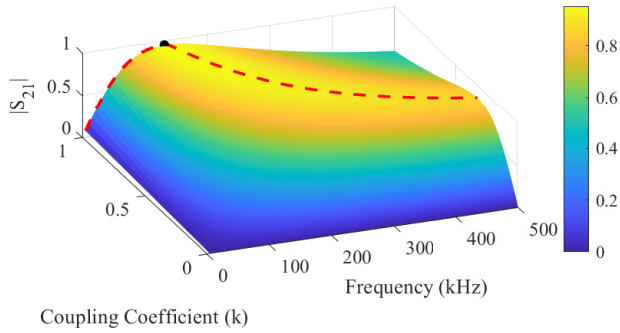


Fig. 6. Dependence of  $|S_{21}|$  on frequency and coupling coefficient.

enhancement provides a practical means to maintain efficient power transfer in a wider range of operational conditions.

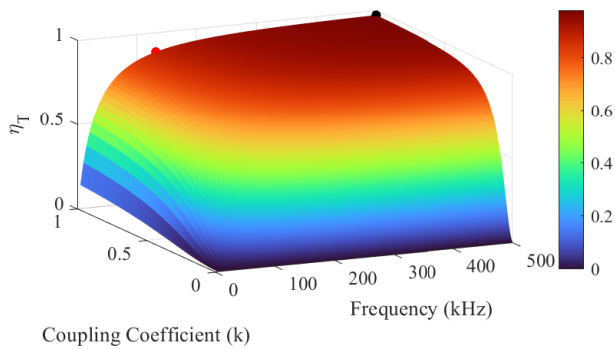


Fig. 7. Dependence of  $\eta_T$  on frequency and coupling coefficient.

Figure 7 shows a prominent peak in the red region, indicating maximum transfer efficiency at high coupling coefficients and relatively low frequencies. Two critical points are highlighted: the red dot marks the highest efficiency at the system's designed resonance frequency of 131.31 kHz, while the black dot indicates the global maximum efficiency which occurs at 500 kHz in a perfect coupling scenario. Figure 8, which is an X-Y view of Figure 7, further provides valuable information, such as the dashed cyan line, marking the resonance frequency, showing how the efficiency decreases with lower values of  $k$ .

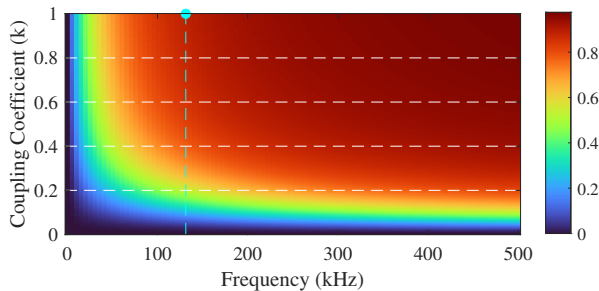


Fig. 8. X-Y view of Figure 7

In particular, the distinction between the resonant frequency

optimum and the global maximum suggests that achieving optimal performance requires adjusting the operating frequency based on the coupling scenario and transfer distance. The horizontal white lines offer a clear visualisation of the efficiency trend: as frequency increases for lower coupling coefficients, the colour gradient transitions from greens and yellows towards red, indicating improved efficiency.

### III. CONCLUSION

The analysis of fractional-order WPT systems through scattering parameters reveals several significant advantages over classical WPT systems. The most notable improvement is the variable nature of  $k_{critical}$  in fractional systems compared to the fixed value in classical systems. While the classical WPT system maintains a constant  $k_{critical}$  of 1.0 across all frequencies, the fractional system exhibits a frequency-dependent one, offering greater operational flexibility. This adaptive characteristic of the fractional system provides two key benefits;

- 1) *Enhanced distance adaptability* - The system can maintain optimal power transfer efficiency at various distances by adjusting the operating frequency, rather than being constrained by a fixed coupling coefficient.
- 2) *Broader operational range* - The frequency-dependent  $k_{critical}$  allows efficient power transfer even in scenarios where achieving perfect coupling is impractical or impossible.

The  $S_{21}$  parameter-based analysis demonstrates that the fractional system achieves high transmission coefficients across a wider range of coupling coefficients, particularly when operating at higher frequencies. This contrasts with the classical system, which shows optimal performance only under near-perfect coupling conditions and within a narrow frequency band around the resonant frequency. Furthermore, the efficiency analysis reveals that the fractional system maintains higher transfer efficiency at lower coupling coefficients by leveraging higher frequency operations, a capability not present in classical WPT systems. This characteristic is particularly valuable for real-world applications where maintaining perfect coupling is challenging due to spatial constraints or movement between the transmitter and receiver.

These findings suggest that fractional-order WPT systems offer superior adaptability and practical utility compared to their classical counterparts, particularly in applications that require variable transfer distances or dealing with coupling limitations. The ability to optimise performance through frequency adjustment rather than physical coupling modifications represents a significant advancement in wireless power transfer technology.

### REFERENCES

- [1] Z. Bi, T. Kan, C. C. Mi, Y. Zhang, Z. Zhao, and G. A. Keoleian, "A review of wireless power transfer for electric vehicles: Prospects to enhance sustainable mobility," *Applied Energy*, vol. 179, p. 413–425, Oct. 2016.
- [2] K. Agarwal, R. Jegadeesan, Y.-X. Guo, and N. V. Thakor, "Wireless power transfer strategies for implantable bioelectronics," *IEEE Reviews in Biomedical Engineering*, vol. 10, pp. 136–161, 2017.

- [3] C. Rong, B. Zhang, and Y. Jiang, "Analysis of a fractional-order wireless power transfer system," *IEEE Transactions on Circuits and Systems II: Express Briefs*, vol. 67, no. 10, pp. 1755–1759, 2020.
- [4] R. Prasad, K. Sharma, B. Gulabdas, and U. Mehta, "Model of fractional-order resonant wireless power transfer system for optimal output," *Journal of Electrical Engineering*, vol. 73, pp. 258–266, 09 2022.
- [5] X. Shu and B. Zhang, "The effect of fractional orders on the transmission power and efficiency of fractional-order wireless power transmission system," *Energies*, vol. 11, p. 1774, 07 2018.
- [6] X. Shu, B. Zhang, C. Rong, and Y. Jiang, "Frequency bifurcation in a series-series compensated fractional-order inductive power transfer system," *Journal of Advanced Research*, vol. 25, p. 235–242, 2020.
- [7] Despotović, D. Reljić, V. Vasić, and D. Oros, "Power transfer analysis of an asymmetric wireless transmission system using the scattering parameters," *Electronics*, vol. 10, no. 8, p. 906, 2021.
- [8] R. Prasad, K. Kothari, and U. Mehta, "Flexible fractional supercapacitor model analyzed in time domain," *IEEE Access*, vol. 7, pp. 122626–122633, 2019.
- [9] K. Kothari, U. Mehta, and R. Prasad, "Fractional-order system modeling and its applications," *Journal of Engineering Science and Technology Review*, vol. 12, no. 6, pp. 1–10, 2019.
- [10] R. Prasad, U. Mehta, and K. Kothari, "Fractional impedance of supercapacitor: an extended investigation," *Int. J. Dynam. Control*, vol. 9, p. 1277–1284, 2021.
- [11] M. Bošković, T. B. Šekara, B. Lutovac, M. Daković, P. D. Mandić, and M. P. Lazarević, "Analysis of electrical circuits including fractional order elements," in *2017 6th Mediterranean Conference on Embedded Computing (MECO)*, pp. 1–6, 2017.
- [12] R. Alahmad and A. Abdelhadi, "Introduction to fractional calculus," in *2019 Advances in Science and Engineering Technology International Conferences (ASET)*, pp. 1–5, 2019.
- [13] A. Ali, A. Kumar, U. Mehta, and M. Cirrincione, *Intelligent data-driven approach for fractional-order wireless power transfer system*, p. 218–236. CRC Press, Mar. 2024.
- [14] A. Ali and U. Mehta, "A comprehensive review of wireless power transfer systems: Focused study with fractional-order elements," *International Journal of Circuit Theory and Applications*, vol. 52, no. 7, p. 3664–3678, 2024.
- [15] N. Mijat, D. Jurisic, and G. S. Moschytz, "Analog modeling of fractional-order elements: A classical circuit theory approach," *IEEE Access*, vol. 9, pp. 110309–110331, 2021.
- [16] A. Kartci, N. Herencsar, J. Tenreiro Machado, and L. Brancik, "History and progress of fractional-order element passive emulators: A review," *Radioengineering*, vol. 29, pp. 296–304, 06 2020.
- [17] M. E. Fouda, A. AboBakr, A. S. Elwakil, A. G. Radwan, and A. M. Eltawil, "Simple mos transistor-based realization of fractional-order capacitors," in *2019 IEEE International Symposium on Circuits and Systems (ISCAS)*, pp. 1–4, 2019.
- [18] G. Varshney, N. Pandey, and R. Pandey, *Fractional-Order Capacitor Realization Based upon Active Inductor*, pp. 259–269. 06 2023.
- [19] Z. Shah, M. Kathjoo, F. Khanday, K. Biswas, and C. Psychalinos, "A survey of single and multi-component Fractional-Order Elements (FOEs) and their applications," *Microelectronics Journal*, vol. 84, 12 2019.
- [20] K. Kothari, R. Prasad, and U. Mehta, "Generalized formulation to estimate the supercapacitor's r-c series impedance using fractional order model," *Alexandria Engineering Journal*, vol. 60, no. 6, pp. 5851–5859, 2021.